

LA-UR-21-27974 (Accepted Manuscript)

Growth and characterization of uranium oxide thin films deposited by polymer assisted deposition

Kruk, Izabela Iwona
Watkins, Erik Benjamin
Scott, Brian Lindley
Wolfsberg, Laura Evon

Provided by the author(s) and the Los Alamos National Laboratory (2021-08-16).

To be published in: Thin Solid Films

DOI to publisher's version: 10.1016/j.tsf.2021.138874

Permalink to record: <http://permalink.lanl.gov/object/view?what=info:lanl-repo/lareport/LA-UR-21-27974>

Disclaimer:

Los Alamos National Laboratory, an affirmative action/equal opportunity employer, is operated by Triad National Security, LLC for the National Nuclear Security Administration of U.S. Department of Energy under contract 89233218CNA000001. By approving this article, the publisher recognizes that the U.S. Government retains nonexclusive, royalty-free license to publish or reproduce the published form of this contribution, or to allow others to do so, for U.S. Government purposes. Los Alamos National Laboratory requests that the publisher identify this article as work performed under the auspices of the U.S. Department of Energy. Los Alamos National Laboratory strongly supports academic freedom and a researcher's right to publish; as an institution, however, the Laboratory does not endorse the viewpoint of a publication or guarantee its technical correctness.

Journal Pre-proof

Growth and characterization of uranium oxide thin films deposited by polymer assisted deposition

Izabela Kruk , Brian L. Scott , Erik B. Watkins ,
Laura E. Wolfsberg

PII: S0040-6090(21)00357-6
DOI: <https://doi.org/10.1016/j.tsf.2021.138874>
Reference: TSF 138874



To appear in: *Thin Solid Films*

Received date: 5 November 2020
Revised date: 2 August 2021
Accepted date: 3 August 2021

Please cite this article as: Izabela Kruk , Brian L. Scott , Erik B. Watkins , Laura E. Wolfsberg , Growth and characterization of uranium oxide thin films deposited by polymer assisted deposition, *Thin Solid Films* (2021), doi: <https://doi.org/10.1016/j.tsf.2021.138874>

This is a PDF file of an article that has undergone enhancements after acceptance, such as the addition of a cover page and metadata, and formatting for readability, but it is not yet the definitive version of record. This version will undergo additional copyediting, typesetting and review before it is published in its final form, but we are providing this version to give early visibility of the article. Please note that, during the production process, errors may be discovered which could affect the content, and all legal disclaimers that apply to the journal pertain.

© 2021 Published by Elsevier B.V.

Highlights:

- Polymer assisted deposition produces epitaxial α - U_3O_8 thin film on LSAT substrate
- The thin film stoichiometry determined with diffraction and reflectometry
- Neutron and x-ray reflectometry provide uranium oxide compositional depth profile

Journal Pre-proof

Growth and characterization of uranium oxide thin films deposited by polymer assisted deposition

Izabela Kruk^{1*}, Brian L. Scott¹, Erik B. Watkins¹, Laura E. Wolfsberg²,

¹Materials Physics and Applications Division, Los Alamos National Laboratory, Los Alamos, New Mexico 87545, United States

²Chemistry Division, Los Alamos National Laboratory, Los Alamos, New Mexico 87545, United State

* Corresponding author. Email: iik@lanl.gov

Abstract

A thin film of uranium oxide was deposited by polymer assisted deposition on a single crystal lanthanum aluminate - strontium aluminum tantalate substrate. The deposition resulted in formation of epitaxial thin film of uranium oxide, which could be attributed to α -U₃O₈ or α -UO₃. X-ray diffraction revealed preferential orientation along (100) in case of α -U₃O₈ or (001) for α -UO₃ for the thin film. A combination of x-ray and neutron reflectometry proved the sample to be α -U₃O₈. The film was of 17 nm thickness covered by a capping layer. The less dense capping layer could be a manifestation of surface water adsorbed on the sample.

KEYWORDS: *Uranium oxide; Thin film; X-ray Diffraction; Neutron reflectometry; Polymer assisted deposition; Triuranium octoxide*

1. Introduction

Uranium oxides are of technological importance for the nuclear industry, both in reprocessing of fresh defective fuel and in dry storage of used nuclear fuel. The significance of deposition of uranium oxides as thin films has been growing. It is because thin films are excellent candidates for investigation of radioactive damage, reactions and corrosion products in nuclear fuel [1, 2]. Furthermore, uranium oxide thin films are good catalysts in thermal and photolytic hydrogen production. Their interesting properties, like high reflectivity in the extreme UV region, as well as high dielectric constant make uranium oxide thin films attractive candidates for optical and semiconductor applications [3]-[7].

Vacuum evaporation [8]-[13] sol-gel [6] solution, and magnetron sputtering [3, 4, 14]-[17] techniques have been utilized for depositing of uranium oxide thin films since the 1960s. These

techniques lead to formation of polycrystalline phases. The breakthrough came in 2007 when the first high quality single crystal film of UO_2 was achieved by polymer assisted deposition (PAD) [1, 18, 19]. More recently Elbakhshwan and Heuser reported growth of epitaxial single-crystal-like UO_2 thin films on different substrates by reactive magnetron sputtering [17]. Another example of great synthetic progress has been reported by Chen's group, who applied pulsed laser deposition method to stabilize epitaxial growth of uranium oxides on different substrates [20].

Among many limitations of the studies on uranium based materials none is more critical than the concern of safe handling and storage. From this point of view, polymer assisted deposition is an attractive alternative. PAD is cost effective, non-vacuum method that requires only small amounts of material (tens of mg per 1 cm^2 of the substrate) and can be considered superior to sputtering techniques. The PAD technique is water based and gas phases or flammable solvents are not needed to form metal oxide films. [19] The technique has become valuable for preparation of epitaxial films of hazardous transuranic actinides, for which single crystal materials of high purity are hard to prepare. The PAD method involves complexing uranium ions (or other metal ions) to an aqueous-soluble multidentate polymer, allowing for rapid formation chemical reactions between the metal and the solvent, but also conserves a uniform distribution of the metal in the aqueous solution. [21, 22] The solution is spun and fired at high temperatures to drive off the polymer and form the metal oxide. Structural stability of the metal oxide, even at high temperatures of depolymerisation, is locked by a structurally matching substrate.

The growth of pure single crystals of actinide oxides is complicated by their rich phase diagram [23, 24]. Many of these phases adopt different structural forms, i.e. there are two known polymorphs of U_3O_8 (hexagonal and orthorhombic structures) and at least seven crystalline modifications of UO_3 , of which six can be made at atmospheric pressure. In addition, there are several different products of hydrolysis. Their variety depends on conditions the uranium oxides are subjected to [25]. The most common hydrolysis products of UO_3 are UO_3 monohydrate, $\text{UO}_2 \cdot 2\text{H}_2\text{O}$ (Schoepite) and $(\text{UO}_2)_4\text{O}(\text{OH})_6 \cdot 5\text{H}_2\text{O}$ (meta-Schoepite).

The large volume change upon conversion of UO_2 to UO_3 hydrates creates potential for damage of used fuel with defected cladding. Uranium (VI) species precipitate within a liquid-like film of adsorbed moisture on the UO_2 surface. The mechanism is similar to surface corrosion of iron [26]. Oxygen atoms in U_4O_9 and U_3O_7 , the intermediate phases formed during the oxidation of UO_2 at temperatures of less than $400 \text{ }^\circ\text{C}$ make complex clusters, named cuboctahedrons. A cuboctahedron includes five oxygen interstitials, with one being at the cluster center [23]. These examples show the complexity of microstructure and stability issues among the fuel grade uranium and its compounds. To predict the behavior during aging, storage and recycling of radioactive surplus materials, it is essential to have a complete understanding of relation between structure and properties. The subtleties that govern surface chemistry and

interactions between uranyl materials and the environment under different conditions deserve a special focus [27], [28].

The structural isomers of UO_3 have similar thermodynamic stability and most tend to hydrolyze under open atmospheric conditions. That is why mixtures of UO_3 phases and the hydrolysis products are common [29]. The matter complicates the fact of metastability of the uranyl phases and strong phase relationships between U_3O_8 and UO_3 , which contributes to frequent coexistence of their polymorphs [30]. The PAD technique provides a way to stabilize a particular valence state through a choice of a single crystal substrate. In this work we intend to study growth and to characterize less common uranium-oxygen system prepared by polymer assisted deposition. Surface and sub-surface layers of PAD films have not been investigated structurally to ascertain whether additional oxidation or hydration is present. We aim to obtain a deeper understanding of the structural properties of PAD deposited uranium oxide film and its surface layers by x-ray diffraction and a combination of surface sensitive techniques like x-ray and neutron reflectometry. Once the surface structures and speciation of the film are determined a better understanding of reaction in these type of materials will be realized.

2. Experimental section

2.1. *Film growth*

We deposited the uranium oxide thin film using polymer assisted deposition. Our choice was to use the PAD technique in an attempt to stabilize one of the polymorphs on (100) $(\text{La}_{0.18}\text{Sr}_{0.82})(\text{Al}_{0.59}\text{Ta}_{0.41})\text{O}_3$ (LSAT) single crystal substrate, supplied by MTI Corporation, USA. The LSAT substrate offers good phase scattering contrast for both x-ray and neutron reflectometry. The substrate has similar lattice parameters to another substrate used for stabilization of uranium oxide phases, c-cut sapphire. [4] The precursor for the uranium oxide film was 0.3 M aqueous solution of $\text{UO}_2(\text{NO}_3)_2$, which is used when reprocessing fuel. The salt was added to polyethylenimine (PEI) mixed with ethylenediaminetetraacetic acid (EDTA) without adjusting pH. In the last step, the sample was heated to drive off the polymer and form the epitaxial film. The polymer mixture was prepared by combining 2 g PEI with 2 g EDTA and 10 g nanopure water (18.3 Meg-Ohm). The resulting film precursor coating solution was formed by adding 0.3 M $\text{UO}_2(\text{NO}_3)_2$ to bring the U concentration to 70 g/L. Approximately 35 μL of the coating solution was applied onto a single crystal 1 cm^2 substrate and spun at 2500-3000 rpm for 20-30 s on a ChematTechnology Spin-coater (KW-4A) to yield a precursor polymer film. In the next step, the precursor film on substrate was heated, allowing for depolymerization of the PEI to $\text{NH}_2\text{CH}=\text{CH}_2$ and thermal decomposition of the EDTA to acetic acid, formic acid and ethylenediamine, accompanied by epitaxial growth of uranium oxides on the substrate [21]. Depolymerization, elimination of organic constituents, and formation of the film was conducted in air at 1000 $^\circ\text{C}$ for 3 h by ramping to 120 $^\circ\text{C}$ at 1 $^\circ\text{C}/\text{min}$; holding for 1 h; ramping to 350 $^\circ\text{C}$ at 1 $^\circ\text{C}/\text{min}$; holding for 1 h; ramping to 1000 $^\circ\text{C}$ at 1 $^\circ\text{C}/\text{min}$; holding for 3 h and then cooling to room temperature.

2.2. X-ray and neutron reflectometry

The reflectometry method relies on reflectivity, defined as the ratio of the number of particles elastically and specularly scattered from a surface and interfaces to that of the incident beam. When measured as a function of wave-vector transfer Q_z

($Q_z = |k_{out} - k_{in}| = \frac{4\pi \sin \theta}{\lambda}$, where θ is the angle of incidence and λ is the wavelength of the beam), the reflectivity curve contains information regarding the sample-normal profile of the

in-plane average of the scattering length density SLD ($SLD = \frac{\sum_{i=1}^n b_{ci}}{V_m}$, where b_{ci} is the bound scattering length of i -th of n atoms in a molecular volume V_m) and is finely suited for studies of thin films. Each material that is present in a thin film sample has its own characteristic refraction index, correlated with SLD , which allows the determination of sample composition.

The PAD film was analyzed with x-ray reflectometry (XRR) and x-ray diffraction (XRD) using a Bruker D8 diffractometer with Bragg-Brentano geometry employing $\text{Cu K}\alpha$ radiation of wavelength 1.54056 Å. The beam was conditioned using a Göbel mirror to provide a beam divergence of 0.008°, and reduction of $\text{K}\alpha_2$ and $\text{K}\beta$ contributions. Specular reflection from the film surface and film-substrate interface were collected with NaI scintillator detector. Neutron reflectometry (NR) measurements were carried out using the Asterix time-of-flight (TOF) reflectometer at the Manuel Lujan Jr. Neutron Scattering Center, Los Alamos National Laboratory. The neutron beam is produced from a spallation source and, after moderation by liquid hydrogen, directed onto the sample at low angles. Specular reflection from the sample surface is recorded by a TOF, position-sensitive detector. Neutron wavelengths ranged from 4.5 to 13 Å, and the Q_z -range was covered by measurements performed at different angles of incidence (i.e., 0.5, 1.0, 2.0°). Intensities were collected over the range $0.01 < Q_z < 0.2 \text{ \AA}^{-1}$, background subtracted, and normalized to unity. Unlike in the case of x-rays, the coherent neutron scattering length, b , is not a monotonic function of the atomic number, Z , of elements. In the case studied here, the value of b for oxygen is of comparable magnitude to the values for uranium. As a result, neutrons are a powerful probe to study the oxygen distribution in high Z uranium oxide films. It is important to note that, since reflectivity data are normalized to the incident intensity under conditions of total external reflection, the measured SLD values are absolute and do not need to be arbitrarily scaled.

Analysis of the XRR and NR was performed by fitting the reflectivity profile of a real-space model to the measured reflectivity curve using box models that implement the Abeles matrix

formalism [31]. The modelling was executed using the MOTOFIT software package [32], which allowed determination of film thickness, density, interfacial and surface roughness.

2.3. Thin film X-ray diffraction (t-XRD):

Identification of thin film phases was performed with x-ray diffraction method on a Bruker D8 Discover diffractometer equipped with monochromatic Cu K_{α} radiation, which operated at 40 kV and 40 mA. The diffractometer operated with the Bragg-Brentano geometry. The x-rays were conditioned with a one-quarter Göbel mirror to 0.008 ° in divergence, and measured using a NaI scintillation detector. The t-XRD measurements were performed using 0.1 mm (incident beam) and 0.2 mm (detector side) slits. X-ray diffraction from epitaxial thin films yields peaks arising only from the lattice planes parallel to the film surface and the substrate. Nonetheless, diffraction profiles allow phase indexing, giving information on phase composition. The epitaxial nature of the films was also investigated by the t-XRD technique. A rocking curve scan was performed on the well defined peak of the deposited uranium oxide. This allowed determine the mosaic spread within epitaxial film, with larger full width half maximum (FWHM), correlating with increased mosaicity.

3. Results and Discussion

A thin film of uranium oxide was deposited on a single crystal of (100) $(La_{0.18}Sr_{0.82})(Al_{0.59}Ta_{0.41})O_3$ LSAT substrate. The LSAT lattice is cubic [33], with a unit cell dimension of 3.868 Å, and provides lattice match for two UO_x phases: orthorhombic $\alpha-UO_3$ ($a = 3.961$ Å, $b = 6.860$ Å, $c = 4.167$ Å, $C2mm$) [34] and $\alpha-U_3O_8$ ($a = 4.148$ Å, $b = 11.97$ Å, $c = 6.717$ Å, $Amm2$) [35]. An examination of the crystal structures show many instances of lattice match between the LSAT a-axis and lattice constants in $\alpha-U_3O_8$ and $\alpha-UO_3$ (Figure 1). These lattice matches range from 2-13%, and provide a suitable template for uranium oxide film growth. For $\alpha-U_3O_8$, one unit cell would occupy an ab square of 2x3 LSAT unit cells. For $\alpha-UO_3$, one unit cell would occupy an ab square of 1x2 LSAT unit cells. The t-XRD shows the deposited film planes have an orientation that is normal to the a-axis and c-axis for $\alpha-U_3O_8$ and $\alpha-UO_3$, respectively (Figure 2). The presence of only the (100) and (001) peaks in $\alpha-U_3O_8$ and $\alpha-UO_3$, respectively, demonstrate at minimum a high degree of preferred orientation and possible in plane alignment of the films due to lattice matching (*vide supra*). Moreover, the lattice constant that shows the poorest lattice match for each phase is perpendicular to the plane of the film, which is an additional indication that lattice matching is a factor for possible plane epitaxy. The (100) Bragg peak of $\alpha-U_3O_8$ and the (001) Bragg peak of $\alpha-UO_3$ both fall within the broad profile of the measured film diffraction peak. The $\alpha-U_3O_8$ peaks are a closer match to the measured peak center, especially for the higher order reflections. But the x-ray diffraction is not conclusive as to which of these two phases is present, and the discussion now turns to

determine the phase. The peak shape of the x-ray diffraction spectrum is affected by a use of copper foils. The foils help to optimize signal from the sample. In case of very high intensities of uranium containing phases the signal has been cut off before reaching maximum by the foil in order to protect the detector.

X-ray and neutron reflectometry complemented phase evaluation via x-ray diffraction. The techniques offer a different contrast between the substrate and the phases of the deposited film. This feature is valuable when dealing with challenging materials, like uranium oxides. Frequently, the composition of these materials is not stoichiometrically precise and their oxide structures change under different environmental conditions. Using neutrons provides additional advantage in structural characterization of hydrides and oxides of heavy metals, because they can easier detect the lighter elements, such as H/D and O, within the actinide matrices [36]. Figure 3 illustrates neutron and x-ray scattering length densities for different uranium oxide phases, showing that reflectometry is able to distinguish between them.

To obtain precise structural information, NR and XRR data were analyzed using models. The models describe the measurement as a series of boxes each parameterized by appropriate neutron and x-ray scattering densities (for α - U_3O_8 and α - UO_3 phases), layer thickness, and interfacial roughness. The roughness is determined by an error function centered between adjacent interfaces. A Levenburg-Marquardt minimization algorithm was used to vary the box model parameters in order to obtain the solution corresponding to the lowest χ^2 value. Typical reduced values for the fits presented were less than 10. In general, our approach used the simplest possible models to describe the data. A two-layer models describing the UO_x and the capping layer were able to reproduce the observed NR and XRR measurements. Table 1 presents properties of the fabricated uranium oxide films, obtained from NR and XRR models.

Figures 4 and 5 show XRR and NR reflectivity measurements (symbols with error bars) together with the fits (solid lines) obtained using the numerical models. Thickness of the uranium oxide film was determined to be 17-18 nm, depending on the method. Fits of the reflectivity data indicate a duplex structure of the film with the dominant uranium oxide phase covered by a thin capping layer of lower scattering length density. Calculated neutron SLD and x-ray SLD of the bottom layer equal $4.41 \pm 0.01 \cdot 10^{-6} \text{ \AA}^{-2}$ and $55.0 \pm 0.04 \cdot 10^{-6} \text{ \AA}^{-2}$ respectively. Theoretical SLD values for α - UO_3 with density of 7.25 g/cm^3 [34], [37] are: n-SLD α - $\text{UO}_3 = 3.94 \cdot 10^{-6} \text{ \AA}^{-2}$ and x-ray-SLD α - $\text{UO}_3 = 47.7 \cdot 10^{-6} \text{ \AA}^{-2}$, whereas, in case of α - U_3O_8 with density of 8.39 g/cm^3 [35] they are: n-SLD α - $\text{U}_3\text{O}_8 = 4.3 \cdot 10^{-6} \text{ \AA}^{-2}$ and x-ray-SLD α - $\text{U}_3\text{O}_8 = 54.9 \cdot 10^{-6} \text{ \AA}^{-2}$. By comparing the theoretical and model values of SLD (refer to table 1), we could ascertain the thin film to be α - U_3O_8 .

No signs of interdiffusion were observed through the film-substrate interface, indicated by the very low calculated roughness. However, the surface of the film, the top 3-4 nm, exhibits reduced scattering length density. Neutron and x-ray scattering length densities for the top layer are: n-SLD = $3.20 \pm 0.02 \cdot 10^{-6} \text{ \AA}^{-2}$ and x-ray-SLD = $45.5 \pm 0.02 \cdot 10^{-6} \text{ \AA}^{-2}$. These values correspond to the theoretical SLDs of UO_3 monohydrate ($d = 6.73 \text{ g/cm}^3$ [25, 38]; n-SLD = 3.22

$\cdot 10^{-6} \text{ \AA}^{-2}$ and x-ray-SLD = $45.5 \cdot 10^{-6} \text{ \AA}^{-2}$). This may suggest the capping layer was formed as a result of partial phase transformation between $\alpha\text{-U}_3\text{O}_8$ and $\alpha\text{-UO}_3$ when some surface water was captured. Presence of water on the surface of the film is probable, because UO_x phases easily accept water molecules to create hydrates [25, 39]. The adsorption of water could have occurred during the five months gap between the reflectivity measurements (May 2019 for XRR and October 2019 for NR); the sample was not stored in any controlled environment and was exposed to air. On the other hand, this gradual decrease in films density, which reaches 76% of bulk density at the air interface may also suggest presence of defects, voids, or other structural imperfections on the film's surface. The differences in film thickness, resulting from comparison XRR and NR data fitting models, are less than 2 nm. They can be explained by different elemental sensitivities of the two methods. Thin films prepared by PAD may be contaminated by carbon due to environmental contamination. But in such a case, one would also expect higher SLD values of the capping layer, if traces of carbon and its compounds with uranium were to affect the film thickness. This is not the case.

Full width at half maximum of a rocking curve determines the mean spread of mosaic crystal, which translates to epitaxial quality of the film. The FWHM of the rocking curve from the (100) reflection of $\alpha\text{-U}_3\text{O}_8$, shown in figure 6, illustrates a good level of crystallinity in the sample along the (100) direction. The FWHM is $0.038 \pm 0.0074^\circ$ or $136.8 \pm 3.6''$, indicative of low mosaic spread of crystallites, and suggestive of a small number of defects and inhomogeneities in the bulk U_3O_8 lattice.

In x-ray diffraction analysis of powder samples and thin films, diffraction peak width provides estimation of crystallite size, based on Scherrer equation. [40] In case of the $\alpha\text{-U}_3\text{O}_8$ thin film, the fit to the Scherrer equation gives a crystallite size of $11.3 \pm 0.06 \text{ nm}$. The fit was obtained for the (100) peak and corresponds to the film thickness.

4. Summary

In this work we report about structural characterization of uranium oxide thin films deposited by PAD on $(\text{La}_{0.18}\text{Sr}_{0.82})(\text{Al}_{0.59}\text{Ta}_{0.41})\text{O}_3$. The PAD growth of the material resulted in a single crystal structure quality films of $\alpha\text{-U}_3\text{O}_8$ with a preferred orientation (100). This result is based on XRD, which indicates formation of either $\alpha\text{-UO}_3$ or $\alpha\text{-U}_3\text{O}_8$, with a better correspondence to $\alpha\text{-U}_3\text{O}_8$. XRR and NR confirmed that the film is $\alpha\text{-U}_3\text{O}_8$ indeed. This study provides strong evidence for the formation of $\alpha\text{-U}_3\text{O}_8$ phase stabilized by LSAT substrate.

Declaration of Competing Interest

The authors declare no competing financial interests or personal relationships that could have appeared to influence the work reported in this paper.

Author Contributions

The manuscript was written through contributions of all authors. All authors have given approval to the final version of the manuscript.

Acknowledgments

This work was supported by the US Department of Energy through the Los Alamos National Laboratory. Los Alamos National Laboratory is operated by Triad National Security, LLC, for the National Nuclear Security Administration of U.S. Department of Energy (Contract No. 89233218CNA000001). This work benefited from the use of the time-of-flight neutron reflectometer (Asterix) at the Lujan Neutron Scattering Center at LANSCE.

Data availability

The raw/processed data required to reproduce these findings cannot be shared at this time due to technical or time limitations.

References

- [1] S. R. Qiu, C. Amrhein, M. L. Hunt, R. Pfeffer, B. Yakshinskiy, L. Zhang, T.E. Madey, J. A. Yarmoff, Characterization of uranium oxide thin films grown from solution onto Fe surfaces, *Appl. Surf. Sci.* 181 (2001) 211–224.
- [2] P. B. Weisensee, J. P. Feser, D. G. Gahill, Effect of ion irradiation on the thermal conductivity of UO_2 and U_3O_8 epitaxial layers, *J. Nucl. Mater.* 443 (2013) 212–217.
- [3] J. Lin, I. Dahan, B. Valderrama, M. Manue, Structure and properties of uranium oxide thin films deposited by pulsed dc magnetron sputtering, *Appl. Surf. Sci.* 301 (2014) 475–480.
- [4] M. M. Strehle, B. J. Heuser, M. S. Elbakhshwan, X. C. Han, D. J. Gennardo, H. K. Pappas, H. Ju, Structure and properties of uranium oxide thin films deposited by pulsed dc magnetron sputtering, *Thin Solid Films* 520 (2012) 5616–5626.
- [5] G. J. Hutchings, C. S. Heneghan, I. D. Hudson, S. H. Taylor, Uranium-oxide-based catalysts for the destruction of volatile chloro-organic compounds, *Nature* 384 (1996) 341–343.
- [6] T. T. Meek, B. von Roedern, P. G. Clem, R. J. Hanrahan, Some optical properties of intrinsic and doped UO_2 thin films, *Mater. Lett.* 59 (2005) 1085–1088.
- [7] I. A. Artioukov, R. M. Fechtchenko, A. L. Udovskii, Experimental research of stability of thin films on the basis of depleted uranium as reflecting coating for wavelength of 4.5 nm, *Nucl. Instrum. Methods Phys. Res. Sect. A* 575 (2007) 248–250.

- [8] T. K. Bierlein, B. Mastel, Damage in UO_2 Films and Particles during Reactor Irradiation, *J. Appl. Phys.* 31 (1960) 2314–2315.
- [9] F. Vasiliu, V. Topa, N. Pogrion, M. Birjega, Electronmicroscopical Studies of UO_2 Thin Films Evaporated on NaCl Substrates with Colloidal Centres, *Jpn. J. Appl. Phys.* 13 (1974) 605–607.
- [10] S. Steeb, Elektronenbeugungs-untersuchung an einkristallinen schichten von uranoxyden im bereich von UO_2 bis U_4O_9 , *J. Nucl. Mater.* 3 (1961) 235–236.
- [11] S. Steeb, P. Mitsch, Bestimmung der Zwischengitterverteilung von Sauerstoffatomen mittels Elektronenbeugung an einkristallinen Uranodioxydschichten, *J. Nucl. Mater.* 15 (1965) 81–87.
- [12] E. Horl, P. Heilmann, Epitaxial growth of UO_2 on graphite, *J. Nucl. Mater.* 21 (1967) 96–98.
- [13] N. Popescu-Pogrion, F. Vasiliu, M. Birjega, The structure of vacuum-evaporated UO_2 thin films, *J. Nucl. Mater.* 51 (1974) 255–260.
- [14] B. Navinsek, Epitaxial growth of UO_2 thin films produced by cathode sputtering, *J. Nucl. Mater.* 40 (1971) 338–340.
- [15] F. Miserque, T. Gouder, D. H. Wegen, P. D. W. Bottomley, Use of UO_2 films for electrochemical studies, *J. Nucl. Mater.* 298 (2001) 280–290.
- [16] Q. Chen, X. Lai, B. Bai, M. Chu, Structural characterization and optical properties of UO_2 thin films by magnetron sputtering, *Appl. Surf. Sci.* 256 (2010) 3047–3050.
- [17] M. S. Elbakhshwan, B. J. Heuser, Structural and compositional characterization of single crystal uranium dioxide thin films deposited on different substrates, *Thin Solid Films* 636 (2017) 658–663.
- [18] Q. X. Jia, T. M. McCleskey, A. K. Burrell, Y. Lin, G. Collis, H. Wang, A. D. Q. Li, S. R. Foltyn, Polymer-assisted deposition of metal-oxide films, *Nat. Mater.* 3 (2004) 529–532.
- [19] B. Scott, J. Joyce, T. Durakiewicz, R. Martin, T. McCleskey, E. Bauer, H. Luo, Q. Jia, High quality epitaxial thin films of actinide oxides, carbides, and nitrides: Advancing understanding of electronic structure of f-element materials, *Coord. Chem. Rev.* 266–267 (2014) 137–154.
- [20] E. Enriquez, G. Wang, Y. Sharma, I. Sarpkaya, Q. Wang, D. Chen, N. Winner, X. Guo, J. Dunwoody, J. White, A. Nelson, H. Xu, P. Dowden, E. Batista, H. Htoon, P. Yang, Q. Jia, A. Chen, Structural and Optical Properties of Phase-Pure UO_2 , $\alpha\text{-U}_3\text{O}_8$, and $\alpha\text{-UO}_3$ Epitaxial Thin Films Grown by Pulsed Laser Deposition, *ACS Appl. Mater. Interfaces* 12, 31 (2020) 35232–35241
- [21] T. M. McCleskey, E. Bauer, Q. Jia, A.K. Burrell, B. L. Scott, S. D. Conradson, A. Mueller, L. Roy, X. Wen, G. E. Scuseria, R. L. Martin, Optical band gap of NpO_2 and PuO_2 from optical absorbance of epitaxial films, *J. Appl. Phys.* 113 (2013) 013515-1–013515-5.
- [22] A. K. Burrell, T. M. McCleskey, Q. X. Jia, Polymer assisted deposition, *Chem. Commun.* 11 (2008) 1271–1277.
- [23] L. Desgranges, G. Baldinozzi, G. Rousseau, J. C. Niepce, G. Calvarin, Neutron Diffraction Study of the in Situ Oxidation of UO_2 , *Inorganic Chemistry* 48 (2009) 7585–7592.
- [24] D. A. Andersson, G. Baldinozzi, L. Desgranges, D. R. Conradson, S. D. Conradson, Density Functional Theory Calculations of UO_2 Oxidation: Evolution of UO_{2+x} , U_4O_{9-y} , U_3O_7 , and U_3O_8 , *Inorganic Chemistry* 52 (2013) 2769–2778.
- [25] V. J. Wheeler, R. M. Dell, E. Wait, Uranium trioxide and the UO_3 hydrates, *Polyhedron* 26 (1964) 1829–1845.
- [26] P. Taylor, D. D. Wood, A. M. Duclos, D. G. Owen, Formation of uranium trioxide hydrates on UO_2 fuel in air-steam mixtures near 200°C , *J. Nucl. Mater.* 168(1) (1989) 70–75.

- [27] S. Cohen, M. H. Mintz, S. Zalkind, A. Seibert, T. Gouder, N. Shamir, Water chemisorption on a sputter deposited uranium dioxide film — Effect of defects, *Solid State Ion.* 263 (2014) 39–45.
- [28] P. L. Arnold, Z. R. Turner, Carbon oxygenate transformations by actinide compounds and catalysts, *Nat. Rev. Chem.* 1 (2017) 0002.
- [29] L. E. Sweet, Dallas D. Reilly, D. G. Abrecht, E. C. Buck, D. E. Meier, Y. Su, C. S. Brauer, J. M. Schwantes, R. G. Tonkyn, J. E. Szecsody, T. A. Blake, T. J. Johnson, "Spectroscopic studies of the several isomers of UO_3 ," *Proc. SPIE 8901, Optics and Photonics for Counterterrorism, Crime Fighting and Defense IX; and Optical Materials and Biomaterials in Security and Defense Systems Technology X*, 890107
- [30] H. R. Hoekstra, S. Siegel, The uranium-oxygen system: U_3O_8 - UO_3 , *Inorg. Nucl. Chem.* 1961, 18, 154–165.
- [31] F. Abeles, Sur la propagation des ondes électromagnétiques dans les milieux stratifiés, *Ann. Physic.* 3 (1948) 504–520.
- [32] A. Nelson, Co-refinement of multiple-contrast neutron/X-ray reflectivity data using MOTOFIT, *J. Appl. Crystallogr.* 39 (2006) 273–276.
- [33] MTI Corporation Archives 1994-2013. Retrived from www.mtixtl.com on 02 February 2019
- [34] B.O. Loopstra, E.H.P. Cordfunke, On the Structure of Alpha UO_3 . *Recl. Trav. Chim. Pays-Bas* 85, (1966) 135-142.
- [35] B. O. Loopstra, Neutron diffraction investigation of U_3O_8 , *Acta Cryst.*, 17 (1964) 651–654.
- [36] M. J. Demkowicz, J. Majewski, Probing Interfaces in Metals Using Neutron Reflectometry, *Met.*, (2016) 6(1) 20–37.
- [37] L. E. Sweet, C. H. Henager, S. Y. Hu, T. J. Johnson, D. E. Meier, S. M. Peper, J. M. Schwantes, Investigation of Uranium Polymorphs. PNNL-20951. Richland, WA: Pacific Northwest National Laboratory, 2011. http://www.pnl.gov/main/publications/external/technical_reports/PNNL-20951.pdf
- [38] Ceramic-Matrix Fuels Containing Coated Particles. Proceedings of a Symposium Held at Battelle Memorial Institute#, November 5 and 6, 1962. U.S. Atomic Energy Commission, Division of Technical Information, 1962.
- [39] M.P. Wilkerson, S.C. Hernandez, W.T. Mullen, A.T. Nelson, A.T. Nelson, A.L. Pugmire, B.L. Scott, E.S. Sooby, A.L. Tamasi, G.L. Wagner, J.R. Walensky, Hydration of alpha- UO_3 following storage under controlled conditions of temperature and relative humidity, *Dalton Trans*, 49(30) (2020) 10452–10462.
- [40] P. Scherrer, Bestimmung der Größe und der inneren Struktur von Kolloidteilchen mittels Röntgenstrahlen, *Göttingen Nachrichten* (1918) 98–100

Figure Captions

Fig. 1. Picture showing possible lattice matching between the substrate, LSAT, and two uranium oxide phases: α - U_3O_8 and α - UO_3 . The lattice spacing denoted with yellow brackets match the LSAT lattice constant in the range 2-13%. Dark blue= uranium, light blue= lanthanum/strontium, pink= aluminum/tantalum, and red= oxygen.

Fig. 2. X-ray diffraction data obtained from single deposition of UO_x on LSAT substrate. The inset pictures demonstrate matching between diffraction peaks from the thin film and calculated x-ray diffraction peaks from α - U_3O_8 (red) and α - UO_3 (green) phases, with preferred orientation of (100) and (001) orientation, respectively

Fig. 3. The calculated values of the scattering length density (SLD) for some common phases in uranium-oxide system. The calculations are based on specific densities published in literature [29, 36, 37, 38, 39]. The experimental SLD values measured using NR and XRR are denoted as horizontal lines

Fig. 4. X-ray reflectivity curves (a) and x-ray-SLD profiles (b) for PAD deposition of uranium oxide on LSAT substrate. Fig. 4(a): The green solid line through the data points is the best fit corresponding to the SLD distribution profiles shown in the figure 4b and the numerical values listed in table 1. Fig. 4(b): The figure presents film thickness in Å, as a function of distance from the substrate LSAT interface. Calculated x-ray-SLDs were indicated for LSAT and uranium phases (refer to table 1).

Fig. 5. Neutron reflectivity curves (a) and n-SLD profiles (b) for PAD deposition of uranium oxide on LSAT substrate. Fig. 5(a): The red solid line through the data points is the best fit corresponding to the SLD distribution profiles shown in the figure 5(b) and the numerical values listed in table 1. Fig. 5(b): The figure presents film thickness in Å, as a function of distance from the LSAT substrate interface. Calculated n-SLDs were indicated for LSAT and uranium phases (refer to table 1).

Fig. 6. Thin film-XRD rocking curve for the (100) reflection of α - U_3O_8

Figures

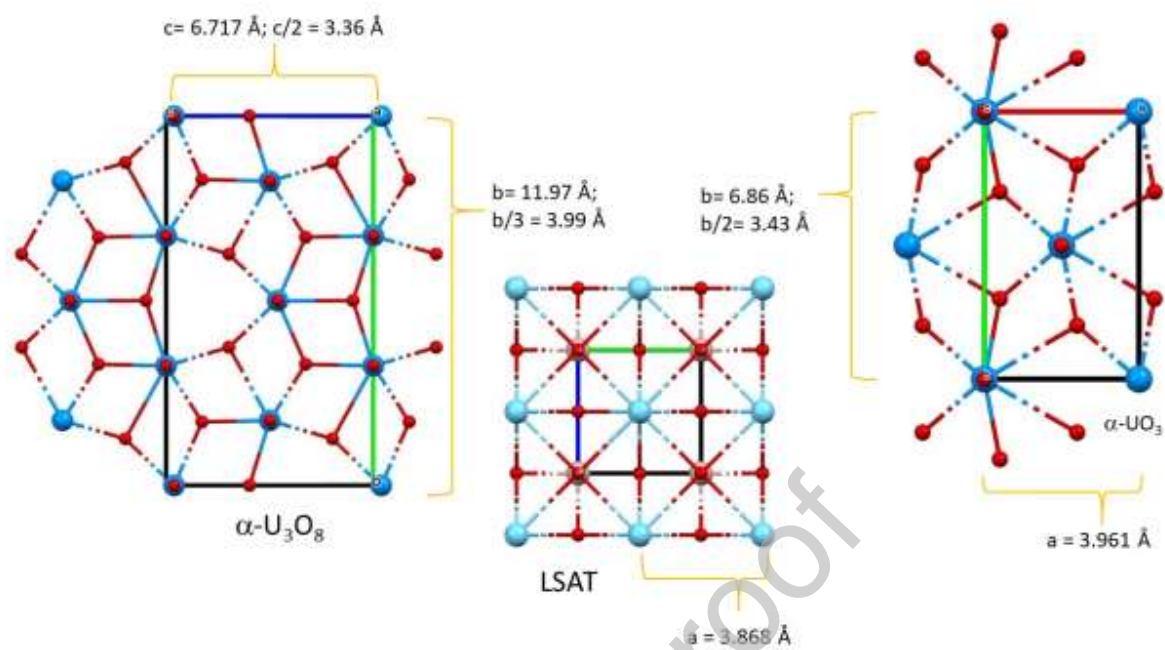


Fig. 1.

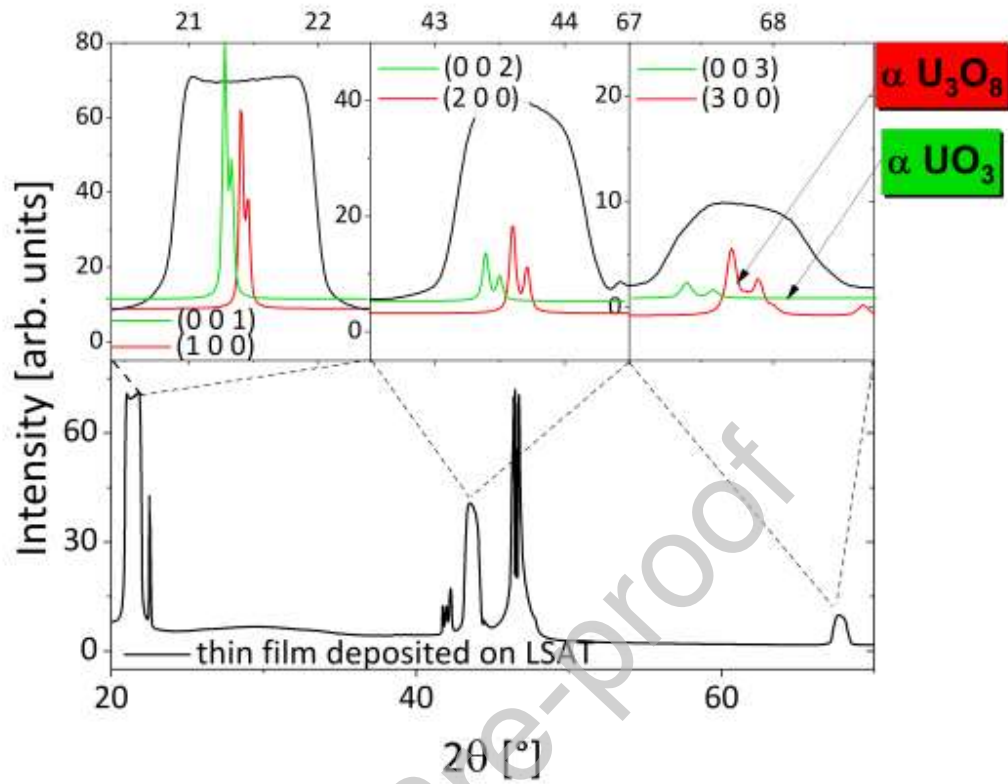


Fig. 2.

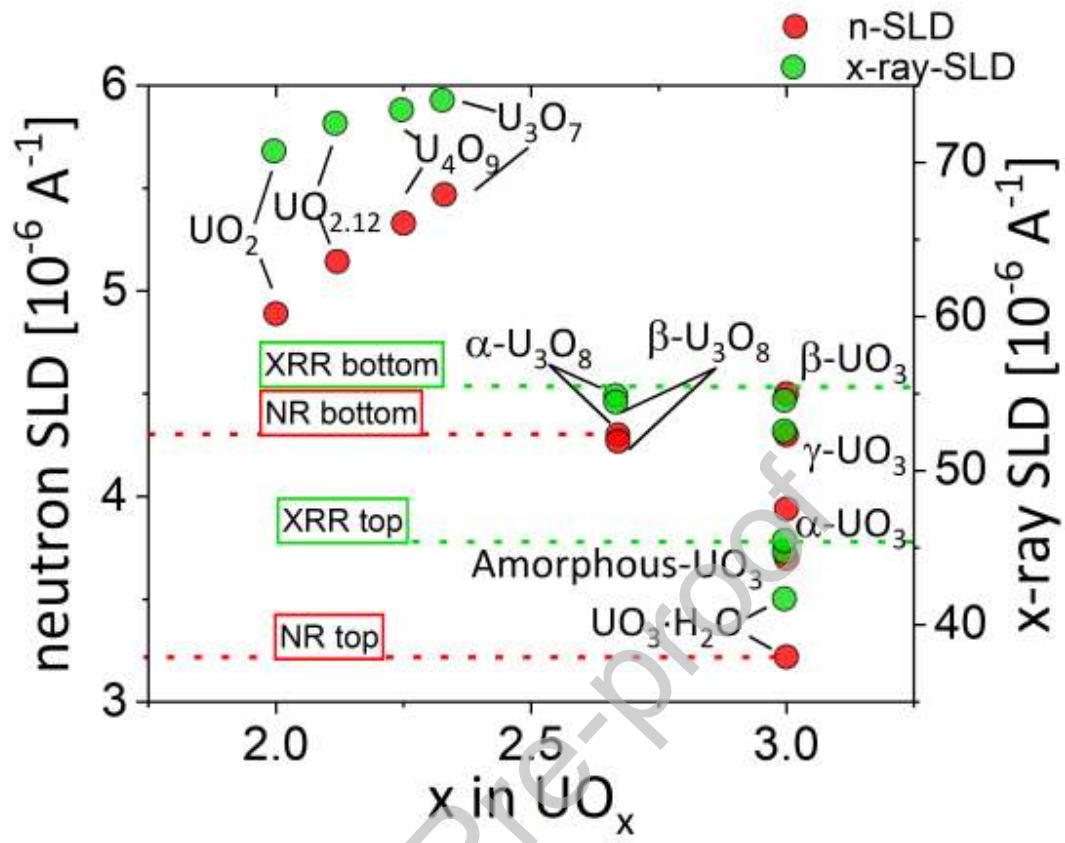


Fig. 3.

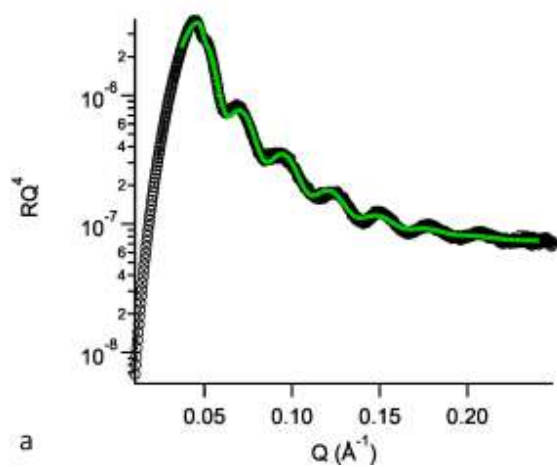


Fig. 4a

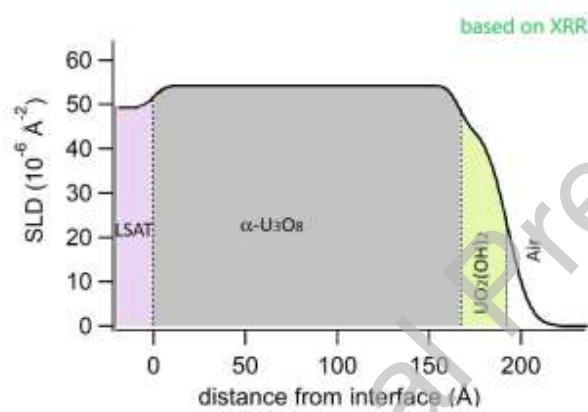


Fig. 4b

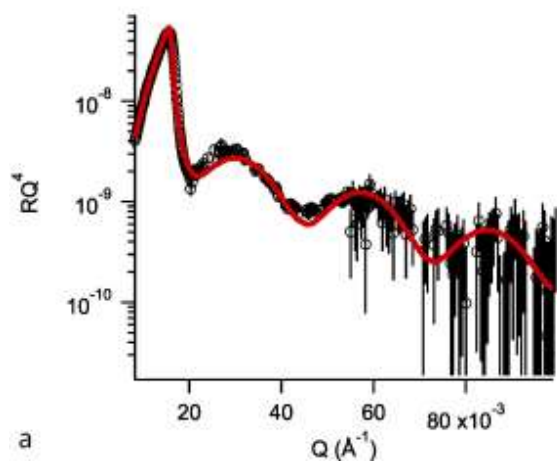


Fig. 5a

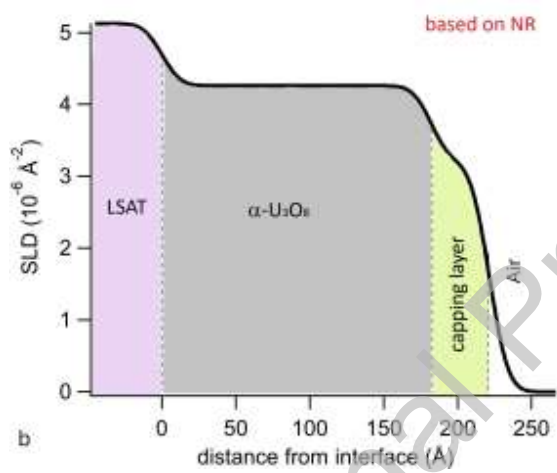


Fig. 5b

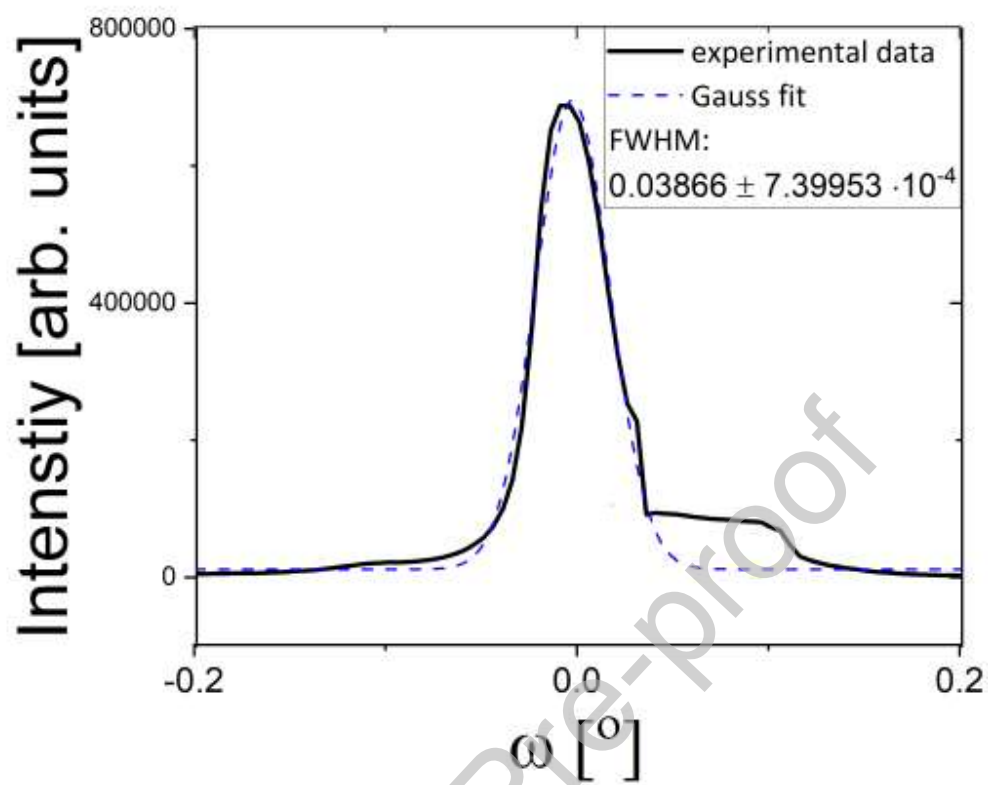


Fig. 6

Table 1: Properties of uranium oxide PAD films grown on the LSAT substrate from XRR and NR data fitting

	Analytical method
--	-------------------

		XRR	NR
Thickness [nm]	Top layer	2.73 ± 0.05	3.92 ± 0.58
	Bottom layer	16.9 ± 0.17	18.2 ± 0.66
Roughness [nm]	UO _x -substrate	1.3 ± 0.12	1.89 ± 0.16
	UO _x -air	0.74 ± 0.0005	0.14 ± 0.20
SLD [$\cdot 10^{-6} \text{\AA}^{-2}$]	Top layer	45.5 ± 0.02	3.20 ± 0.02
	Bottom layer	55.0 ± 0.04	4.41 ± 0.01

Journal Pre-proof